The Astrophysical Journal, 980:123 (7pp), 2025 February 10 https://doi.org/10.3847/1538-4357/ada8a5

The Extreme-ultraviolet Precursors and Postcursors of Solar Flares

Larisza D. Krista[1,2,3]
[1] Cooperative Institute for Research in Environmental Sciences, University of Colorado, Boulder, CO 80309, USA
[2] National Centers for Environmental Information, National Oceanic and Atmospheric Administration, Boulder, CO 80305, USA
[3] Space Science Institute, Boulder, CO 80301, USA
Received 2024 September 28; revised 2024 November 26; accepted 2025 January 7; published 2025 February 7

Abstract

EUV brightenings are small-scale magnetic reconnection events that consistently appear before and after solar flares. However, it is not well understood how EUV precursors might foreshadow flares and what the physical connection is between the EUV signatures and flares. We studied flare-active and inactive periods in three separate studies using the Detection and EUV Flare Tracking (DEFT) tool. In Study 1, EUV signatures were identified in 200 no-flare days, in Study 2 EUV signatures before 360 flares were analyzed, and in Study 3 close to 36,000 EUV signatures were detected, and their pre- and postflare distribution and trends were studied. Our key questions were as follows: do EUV signatures occur consistently before flares, do EUV signatures occur without flares, are there flares without EUV precursors, and is it possible to forecast different magnitude flares based on preceding EUV signature trends? Study 1 showed that in no-flare periods EUV signatures were only detected 4% of the time. Study 2 showed that EUV precursors were present 92% of the time within 6 hr before ⩾C-class flares. Study 3 showed that over 90% of the signatures were associated with flares (⩾B class), and over 50% of all signatures were associated with ⩾M-class flares. A superposed epoch analysis showed precursor frequency peaks at ∼70 and 100 minutes before M- and X-class flares, respectively, while B- and C-class flares had no notable precursor frequency peaks. These results demonstrate the close connection between EUV signatures and flares and the significant potential EUV signatures have in improving space weather forecasting.

Unified Astronomy Thesaurus concepts: Solar flares (1496); Astronomy image processing (2306); Solar extreme ultraviolet emission (1493)

1. Introduction

Solar flares are widely known to be responsible for a multitude of space weather hazards that affect our society. Efforts to forecast solar flares have been ongoing for decades; nevertheless, consistent and reliable solar flare forecasting remains a challenge. In order to predict flares and efficiently forecast space weather, it is necessary to understand flare initiation and the processes that are responsible for triggering solar eruptions. In addition, it is essential to observe and consistently identify signatures that indicate the preflare triggers and the impending flare onset.

Previous findings suggest that chromospheric brightenings correspond to small-scale preflare magnetic reconnection events that can trigger flares (K. Kusano et al. 2020, 2012; Y. Bamba et al. 2013, 2017). K. Kusano et al. (2012) explored different magnetic structures capable of triggering flares. Using 3D magnetohydrodynamic simulations they studied the nonlinear dynamics of a wide variety of magnetic structures and found two types to favor the initiation of solar eruptions. The structures appear near the magnetic polarity inversion lines and include magnetic fluxes reversed to the potential or nonpotential component of the major field. Observations of preflare brightenings in the chromosphere before an X- and M-class flare supported the simulations. K. Kusano et al. (2012) suggest that solar flares are triggered by magnetic disturbances in regions where magnetic shear stores free energy and not by phenomena that occur as a result of free energy storage, i.e., both magnetic shear (or magnetic helicity) and magnetic field disturbance are necessary for flare initiation. K. Kusano et al. (2020) found that magnetic twist flux density near the magnetic polarity inversion line could be used to estimate the time (in the next 20 hr), location, and magnitude of impending flares.

Y. Bamba et al. (2017) investigated how small-scale photospheric changes were related to flares and what chromospheric events occurred in the precursor phase. Precursor brightenings before an X-class flare were analyzed using the Interface Region Imaging Spectrograph (IRIS; B. De Pontieu et al. 2014) and Hinode EUV Imaging Spectrometer (EIS; J. L. Culhane et al. 2007) data. The authors observed a localized jet with a strong precursor brightening, performed spectropolarimetric analysis, and analyzed the photospheric magnetic field and chromospheric/coronal structures using data from the Solar Dynamics Observatory (SDO) Helioseismic and Magnetic Imager (HMI; J. Schou et al. 2024) and the Atmospheric Imaging Assembly (AIA; J. R. Lemen et al. 2023). A significant blueshift was found to be related to a precursor brightening over a characteristic magnetic field structure, which suggests that the flow was accelerated by Lorentz force. The observed large-scale coronal loop structure was connected to the footpoints of the flare ribbons and was destabilized shortly after the precursor brightening. These findings indicate that a small-scale magnetic reconnection occurred in the lower chromosphere and triggered the magnetic reconnection of the X-class flare in the corona.

Using machine learning, N. Nishizuka et al. (2017) developed a model to predict the maximum flare class in the next 24 hr. Data were used from 2010 to 2015, including vector magnetograms, ultraviolet emission, and soft X-ray emission. In all, ∼60 features were extracted with their time differentials

(e.g., magnetic neutral lines, the current helicity, the UV brightening, and the flare history). From the tested machine learning algorithms, the k-nearest neighbors performed best, with a true skill statistic (TSS) of 0.9. Feature importance was found to be in the following order: previous flare activity, magnetic neutral line length, unsigned magnetic flux, area of UV brightening, and time differentials of features over 24 hr. These properties are all strongly correlated with the flux emergence dynamics in an active region (AR). In their follow-up work, N. Nishizuka et al. (2018) used a deep neural network model to calculate the probability of flares in the next 24 hr using binary classification ($\geqslant$M versus $<$ M class or $\geqslant$C versus $<$ C class). Coronal hot brightenings, as well as X-ray and 131 Å intensity data, were added to allow for operational prediction. The authors were able to predict flares with TSS = 0.80 for $\geqslant$M-class flares and TSS = 0.63 for $\geqslant$C-class flares. The authors note that while the prediction process is a black box, the features were manually selected and could be used to analyze which are best for prediction.

In agreement with K. Kusano et al. (2012), H. Wang et al. (2017) argue that the build up of magnetic energy stored in the corona alone may be insufficient to trigger flares, and small-scale energy releases (preflare brightenings, a.k.a. precursors) might be key to understand flare initiation. These precursors are small bipoles, where the magnetic orientation is opposite to the ambient main polarities. The authors studied precursors of a flare using high-resolution data from the New Solar Telescope (W. Cao et al. 2010) and microwave data. They observed two episodes of precursor brightenings at a small-scale magnetic channel near the footpoints of sheared magnetic loops. Microwave spectra showed that the precursor emissions originated in the atmosphere. The results provided evidence of low-atmospheric small-scale energy release that could have been responsible for triggering the main flare.

L. D. Krista & M. Chih (2021) used the Detection and EUV Flare Tracking (DEFT) tool to investigate low-corona signatures, to identify EUV flare precursors in GOES Solar Ultraviolet Imager (SUVI) 304 Å observations. DEFT detects and evaluates simultaneous activities occurring in multiple locations to identify precursor events that indicate impending flares. In a study of 61 flares, they found EUV brightenings consistently occurring within 30 minutes before flare start times. Identifying the last two EUV signatures before the flares, precursors were found to occur earlier for B and C flares and closer to the start times of M- and X-class flares. The study also showed that all magnitude flares (B, C, M, and X class) can have precursors with smaller areas, while only larger (M and X) flares can have larger area signatures. In a follow-up work, L. D. Krista (2025) analyzed the precursor signatures of 351 flares. Across C-, M-, and X-class flares, precursors were detected for 93% of the flares when using a 6 hr window before the flare start times. Using superposed epoch analysis, L. D. Krista (2025) found that elevated precursor activity tends to occur across all magnitude flares in the last 2 hr before the flares. In the last 20 minutes, a significantly higher precursor frequency, pixel count, and power were associated with M-class flares than C-class flares. The author suggests that the observed EUV precursors are the observable signatures of small-scale magnetic reconnection events, and the consistently increasing frequency of precursor activity might indicate increasingly instability, which could lead to flare initiation.

K. D. Leka et al. (2023) used the SDO/AIA Active Region Patch database to find parameters that could identify regions that might produce a flare imminently. Direct and running-difference images were used to perform a nonparametric discriminant analysis and identify rapid brightness changes and long-term intensity evolution. The 94 Å data were found to provide the most parameters with discriminating power. The resulting top Brier Skill Scores (BSS) were in the 0.07–0.33 range, TSS in the 0.68–0.82 range, and the Receiver Operating Characteristic (ROC) skill scores were above 0.8. Using 24 and 6 hr validity periods, they found flare-imminent regions to display short-lived small-scale brightening events.

An increasing number of studies support the hypothesis that solar flares can be initiated by internal magnetic reconnection between small flare-trigger field and the overlying sheared arcade and that such small-scale magnetic reconnection events produce a chromospheric emission that can be observed as preflare brightenings (K. Kusano et al. 2012; Y. Bamba et al. 2017; H. Wang et al. 2017; L. D. Krista & M. Chih 2021; K. D. Leka et al. 2023, L. D. Krista 2025). Our goal is to further explore and expand on these findings using our detection tool and a large-scale analysis of chromospheric brightenings identified in 304 Å observations. We describe the instrument and observations used in our analysis in Section 2 and the EUV signature detection tool in Section 3. We discuss the results in Section 4 and present our conclusions in Section 5.

2. Instrument and Observations

Our EUV signature detection tool uses GOES-R SUVI observations (S. K. Tadikonda et al. 2019; J. P. Fulbright et al. 2017). SUVI is a state-of the art instrument that supports scientific research and space weather forecasting efforts with real-time, high spatial and temporal resolution observations. It is a normal-incidence EUV Ritchey–Chrétien telescope that observes the solar atmosphere in six ultraviolet passbands (93, 131, 171, 195, 284, and 304 Å). The spatial resolution is $2\farcs5$ pixel^{-1}, with a $53\farcm3 \times 53\farcm3$ field of view. The image size is 1280 × 1280 pixels. SUVI operates at a cadence of 10 s, observing the Sun at a variety of wavelengths and exposure times. The SUVI database extends from 2017 to date.

SUVI narrowband observations can be used to distinguish plasma at a wide range of temperatures. Testing our detection tool on all available wavelengths, we found that the chromospheric 304 Å observations are optimally sensitive to flare-related EUV signatures (L. D. Krista & M. Chih 2021). In the main phase of a flare the EUV emission tends to brighten after more energetic emissions (e.g., X-rays), but in the low corona, chromospheric observations show small-scale, high-intensity magnetic reconnection signatures minutes to hours before the eruption (Y. N. Su et al. 2006; K. Kusano et al. 2012; Y. Bamba et al. 2013; H. Wang et al. 2017). These bright signatures are only a few pixels in size, so they do not significantly influence the total solar irradiance. Hence, they might not be detectable in integrated irradiance measurements. Furthermore, SUVI imaging allows us to determine and track the locations and temporal changes in the EUV signatures. Simultaneous signatures can be separated, and changes that indicate an impending flare can be distinguished.

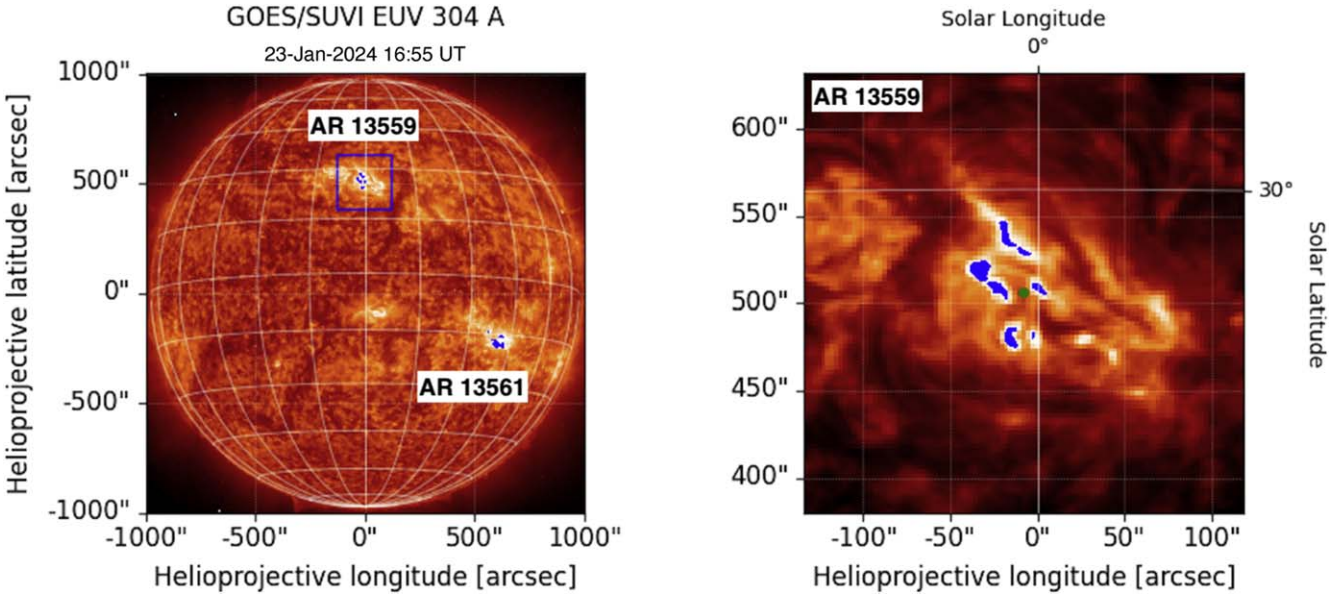

Figure 1. DEFT detection showing ARs 13559 and 13561 and their EUV signatures on 2024 January 23 at 16:55 UT, 37 minutes before a C7.3 flare erupted in AR 13559 at 17:32 UT. The left panel shows the full-disk GOES/SUVI 304 Å observation, highlighting AR 13559 with a blue box. The blue box is shown magnified in the right panel, where the blue pixels show the monitored EUV signatures.

3. Method

The DEFT tool was developed to identify EUV signatures in SUVI observations quickly and consistently with minimal computational overhead (L. D. Krista & M. Chih 2021). Of the six available SUVI wavelengths, we focus on the 304 Å wavelength observations as they efficiently identify flare-related signatures in the transition region/chromosphere ($\leqslant$100,000 K). Furthermore, these observations are available at a temporal cadence of $\sim$2 minutes, which makes them suitable for real-time use.

DEFT is a fully automated tool; using an Apple M2 chip personal computer it takes only a few seconds to analyze a single observation. Therefore, it can process and keep up with incoming real-time GOES/SUVI data. DEFT uses intensity histograms to distinguish EUV signatures and flag those that might be related to flares. The EUV signatures are grouped and tracked in consecutive observations, and their physical properties (heliographic location, EUV intensity, pixel count, and running-difference values) are analyzed and stored. EUV signatures can appear at the same time in different locations; hence, a spatial discriminator was developed to distinguish heliographically separate events. Intensity variations are used to flag signatures that might indicate an impending flare. For more detail, please see L. D. Krista & M. Chih (2021) and L. D. Krista (2025).

An example of DEFT signature detection is demonstrated with flare-producing ARs 13561 and 13559, observed on 2024 January 23. The left panel in Figure 1 shows both ARs in a full-disk SUVI observation at 16:55 UT. DEFT was able to identify and separate activities in both regions throughout the day. The right panel in Figure 1 shows an EUV signal spike in AR 13559 that DEFT correctly flagged as a precursor signature 37 minutes before the C7.3 flare that started at 17:32 UT. DEFT detected another three EUV precursor signatures for this flare in the last 5 minutes before the flare start time.

We take this opportunity to discuss general flare data quality issues we have encountered. We use flare data from 2024 January 23 as an example: NOAA daily flare logs (see *ftp. swpc. noaa. gov/pub/indices/events/*) listed 18 flares for AR 13561, 6 flares for AR 13559, and 2 flares with no ARs on this day. SDO/AIA observations show that the latter two flares occurred in AR 13559. More importantly, SDO/AIA observations also show that the C7.3 (17:32 UT) flare occurred in AR 13559 and not in AR 13561, as shown in the NOAA flare logs. When using the Heliophysics Events Knowledgebase (see https://www.lmsal.com/hek/) and the Python search and retrieval tool *Fido*, we find the NOAA flare entries have no locations or ARs listed, and the last three flares of the day are missing, while the SDO flare database lists more flare events (and sometimes double lists the same flare) than recorded in the NOAA logs. In our current work we mitigate for the discrepancies we discovered by removing multiple listings of the same flare and correcting wrong or missing locations using the SDO/AIA database.

As the above examples demonstrate, multiple regions can be active at the same time. Therefore, for accurate forecasting and documentation it is essential to use observations with spatial data and automated detection tools to distinguish concurrent events and provide a reliable location and timing. We also want to emphasize the urgent need for a thorough revision of currently available flare databases. Reliable and consistent flare location, magnitude, and start-time data are essential for the adequate development, testing, and validation of flare detection tools and models.

4. Results

Three studies were conducted to investigate EUV signatures in flare-active and flare-inactive times. Study 1 includes 200 no-flare days based on NOAA records. The no-flare days were selected from 2017 to date. Furthermore, 6 hr detection windows were used to identify when a no-flare forecast was correct or incorrect. This study investigates the prevalence of EUV signatures in times of prolonged flare inactivity.

Study 2 investigates 360 $\geqslant$C flares and their EUV signatures over 213 nonconsecutive days of data, selected from 2017 to date (solar activity minimum and near maximum). In this data set we include a high number of space-weather-relevant flares:

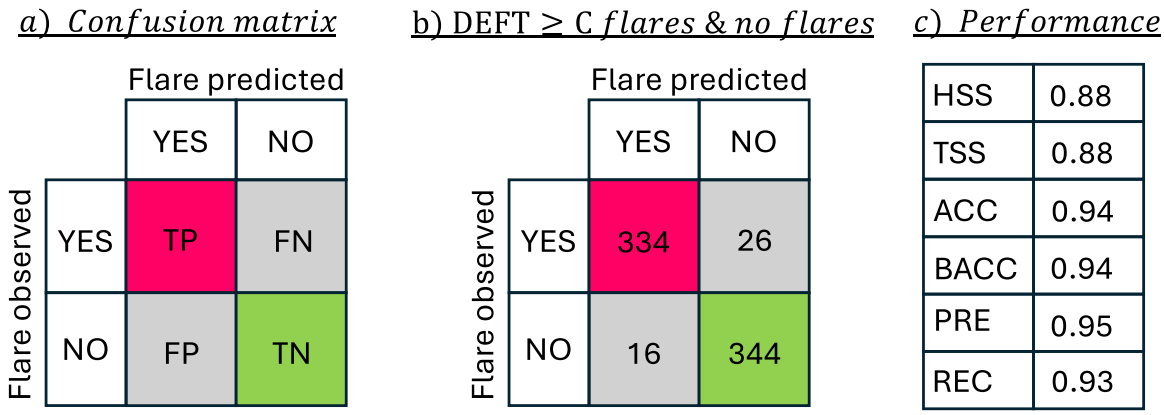

Figure 2. The forecast confusion matrix (a) listing the TP, TN, FN, and FP cases; the corresponding DEFT detection values from Study 1 and 2 (b); and the resulting performance metrics (c).

150 C-, 150 M-, and 60 X-class flares. 6 hr detection windows were used to identify EUV signatures before flares. Forecasts were recorded as correct when signatures were found before flares and incorrect when no signatures were detected. This study investigates whether space-weather-relevant flares are consistently preceded by EUV signatures. Study 1 and 2 were combined to calculate the DEFT tool forecast performance metrics.

In Study 3 all EUV signatures were identified in the 213 days of data (same database as Study 2) and were linked to any class flares, before or after the flare start times. The focus of this study is the EUV signature associations with different magnitude flares and their preflare frequency trends. Note that the analyzed days in the studies are typically nonconsecutive days and were chosen to best target flare-active and flare-inactive investigation. EUV signatures were only associated with flares if they occurred within a 15 heliographic degree radius of a flare location.

4.1. Study 1: No-flare Days

Each day of the analyzed 200-day no-flare data set was split into four 6 hr windows. The first three windows (00:00–18:00) were used as "evaluation windows" to identify any EUV signatures. A 6 hr window the day before (18:00–24:00) and the last window on the no-flare day (18:00–24:00) were used to ensure that no flares occurred before or after the evaluation period. This arrangement resulted in 600 evaluation windows. In three cases flares occurred on nights before. As a result, three windows (00:00–6:00) had to be excluded from the study. In the final data set of 597 windows, 38 signals were detected that were unrelated to any flares. Signals that occurred in the same 6 hr window and in the same location (within 15 heliographic degrees of each other) were regarded as part of the same precursor activity and counted as one incorrect forecast. As a result, the 38 signals accounted for 26 windows, which corresponded to 26 incorrect flare forecasts (false positive, FP). This translates to a 96% correct no-flare forecast (true negative, TN) and 4% false flare forecast (FP) using 6 hr detection windows.

In Study 2 (see next section), 360 6 hr windows were studied. In order to perform our statistical analysis on balanced sample ratios of flare and no-flare data, we had to downsize the Study 1 no-flare database from 597 to 360 windows and proportionally reduce the correct and incorrect forecasts. Our original database consisted of 571 correct and 26 incorrect forecasts, totaling in 597 forecasts. The proportionally reduced data size corresponds to 360 forecasts, consisting of 344 correct no-flare (TN) and 16 incorrect flare forecasts (FP).

4.2. Study 2: 360 Flares and the DEFT Performance Evaluation

In this study 360 flares were analyzed, including C-, M-, and X-class flares. Of the 360 flares, 334 flares were associated with one or more EUV signatures within a 15° radius in a 6 hr window before the flare start time. This translates to 344 correct flare forecasts (true positive, TP). Meanwhile, 26 flares (2 X, 10 M, and 14 C class) had no EUV signatures in the 6 hr window beforehand; hence, these were missed flare forecasts (false negative, FN). This corresponds to a 92% correct flare forecast and an 8% missed flare forecast for ⩾C flares.

We combined Study 1 (no flares) and Study 2 (360 ⩾C flares) to calculate the DEFT forecast performance metrics for the data set. We proportionally downsized the Study 2 data size to the match the 360 forecast windows in Study 1. Combined, they yield the following detection rates: TP (334), FN (26), TN (344), and FP (16). Figure 2 shows the confusion matrix (panel (a)) and the corresponding DEFT detection values (panel (b)).

The following equations were used to calculate the forecast performance metrics:

$$HSS = \frac{2(TP \times TN - FP \times FN)}{(TP + FN)(FN + TN) + (TP + FP)(FP + TN)}, \quad (1)$$

$$TSS = \frac{TP}{TP + FN} - \frac{FP}{FP + TN}, \quad (2)$$

$$ACC = \frac{TP + TN}{TP + TN + FP + FN}, \quad (3)$$

$$BACC = \frac{1}{2}\left(\frac{TP}{TP + FN} + \frac{TN}{TN + FP}\right), \quad (4)$$

$$PRE = \frac{TP}{TP + FP}, \quad (5)$$

$$REC = \frac{TP}{TP + FN}. \quad (6)$$

Here, the Heidke skill score (HSS; P. Heidke 1926) measures the accuracy (ACC) of correct predictions over random chance. The Hanssen and Kuipers discriminant or TSS also evaluates

the forecast performance but without bias when evaluating varying flare/no-flare sample ratios (A. W. Hanssen 1965; A. I. Doswell Charles et al. 1990). For this reason, TSS has been recommended as the standard measure to compare different studies that use different flare/no-flare sample ratios (D. S. Bloomfield et al. 2012). Accuracy (ACC) quantifies the proportion of correct forecasts over all forecasts, while the Balanced Accuracy (BACC) quantifies the averaged rate of correct forecasts. Precision (PRE) corresponds to the accuracy of correct flare predictions over all positive predictions (correct or incorrect), while Recall (REC) quantifies the fraction of flares correctly identified. For more details on evaluation metrics, please see F. Woodcock (1976), D. S. Bloomfield et al. (2012), K. Pelkum Donahue & F. Inceoglu (2024), and references therein.

Using the DEFT tool on a combined database of 360 6 hr preflare windows and 360 6 hr no-flare windows produced the following skill scores: HSS (0.88), TSS (0.88), ACC (0.94), BACC (0.94), PRE (0.95), and REC (0.93). These values are also shown in panel (c) of Figure 2.

The shown performance metrics reflect how well DEFT performs in detecting signatures before ⩾C flares and how often signatures are detected in times of no flare activity. While it is valuable to compare success rates across different flare detection methods, it is important to emphasize that a clear comparison is challenging when the applied methods, detection windows, and event ratios can vary considerably. Nevertheless, the above DEFT skill scores show a significant forecasting potential for EUV signatures.

4.3. Study 3: 35,994 EUV Signatures and Their Flares

This study investigates the same 213 nonconsecutive days that were analyzed in Study 2. Our goal was to identify all signatures and link them to flares as pre- or postcursors. 35,994 EUV signatures were identified over the 213 days of data, and 2,333 flares were cataloged (60 X-, 358 M-, 1453 C-, and 462 B-class flares, according to NOAA logs). Note that events that had no GOES or SDO/AIA location information were excluded from all studies. This is likely the reason why B flare numbers are low in this list. Furthermore, some EUV signatures were related to flares but could not be matched without flare location information; hence, the number of signatures without flares is a conservative estimate.

Signatures were associated with flares within a 15 heliographic degree radius and a ±6 or ±9 hr window. Any signatures without flare associations were also recorded. In this study each EUV signature is associated with only one flare—the largest magnitude flare within the specified detection window. The hierarchical association means that if a B- and M-class flare occurred within a ±6 hr window of a signature, the signature will be associated with the M-class flare based on the hierarchical association. Furthermore, if the B-class flare occurred within ±6 hr of the M-class flare, the EUV signature of the B-class flare itself would also be associated with the M-class flare, i.e., all detected EUV signatures were associated with the highest-magnitude flare within the detection window.

Beyond prioritizing magnitude-based association, signatures were also favored to be assigned as preflare (precursor) over postflare (postcursor) signatures. That is, if two M-class flares occurred within 6 hr of each other (e.g., flare 1 occurred before flare 2), then any signatures that occurred in the time between the two flares would have been assigned as precursors to flare 2 rather than as postcursors to flare 1. The hierarchical association and the precursor-over-postcursor prioritization scheme help us investigate the "activity streak": when brightenings and flares occur in a close location and time to each other. With our association schemes we can follow how activity builds up to the largest flare in the activity streak and then abates over time.

Table 1
Percentage of 35,994 EUV Signatures Associated with Different Magnitude Flares Using the 213 Day Database

Window	X-class Flares (%)	M-class Flares (%)	C-class Flares (%)	B-class Flares (%)	Total Flare Association (%)
± 6 hr	15	39	35	2	91
± 9 hr	19	43	31	1	94
± 6 hr	35	15	39	⋯	89
± 9 hr	31	19	43	⋯	93
± 6 hr	15	39	⋯	⋯	54
± 9 hr	19	43	⋯	⋯	62

Note. The leftmost column lists the detection window size (±6 or ±9 hr). Columns 2, 3, 4, and 5 from the left show the signature association percentages with different magnitude flares. The dashes indicate when lower-class flares were excluded, and their signatures were considered erroneous. The rightmost column shows the total signature–flare association rate for each study.

Table 1 shows the resulting hierarchy-based associations of the identified 35,994 signatures using ±6 and ±9 hr detection windows. The association percentages are also demonstrated when excluding lower-class flares. The leftmost column shows the detection window sizes in each study. Columns 2, 3, 4, and 5 from the left show the percentages of signatures associated with different magnitude flares. Dashes indicate when certain classes of flares were excluded from a study, and the corresponding signatures were considered erroneous, i.e., in the bottom two studies only M- and X-class flares are considered "real flares," and any signatures related to B- or C-class flares were recorded as incorrect detections. The rightmost column ("Total flare association") shows the total signature–flare association rate for each study. The results demonstrate that over 90% of the EUV signatures are associated with ⩾B-class flares and over 50% of the signatures are associated with ⩾M-class flares when using ±6–9 hr detection windows.

Flare–signature associations were also investigated using a superposed epoch analysis, where time "0" is the start time for all included flares. The frequency histograms in Figure 3 demonstrate the EUV signature occurrence frequency before flares. The top panels in Figure 3 show the precursor frequencies in the 2 hr before flares, and the bottom four panels show the precursor frequencies in the 6 hr before flares. Different colors signify different magnitude flares, and X-, M-, C-, and B-class flares are shown from left to right, respectively.

X-class flare precursor signatures showed peaks around 1.2, 2.5, and 3.7 hr before the flare start times. M-class flare precursor signatures showed a frequency peak at around 100 minutes and a gradual increase in the last 50 minutes before the flares. C-class flare precursor frequencies showed a gradual increase without significant peaks. B-class flare precursors showed a lot of small-scale variations relative to their numbers. All magnitude flares showed an overall

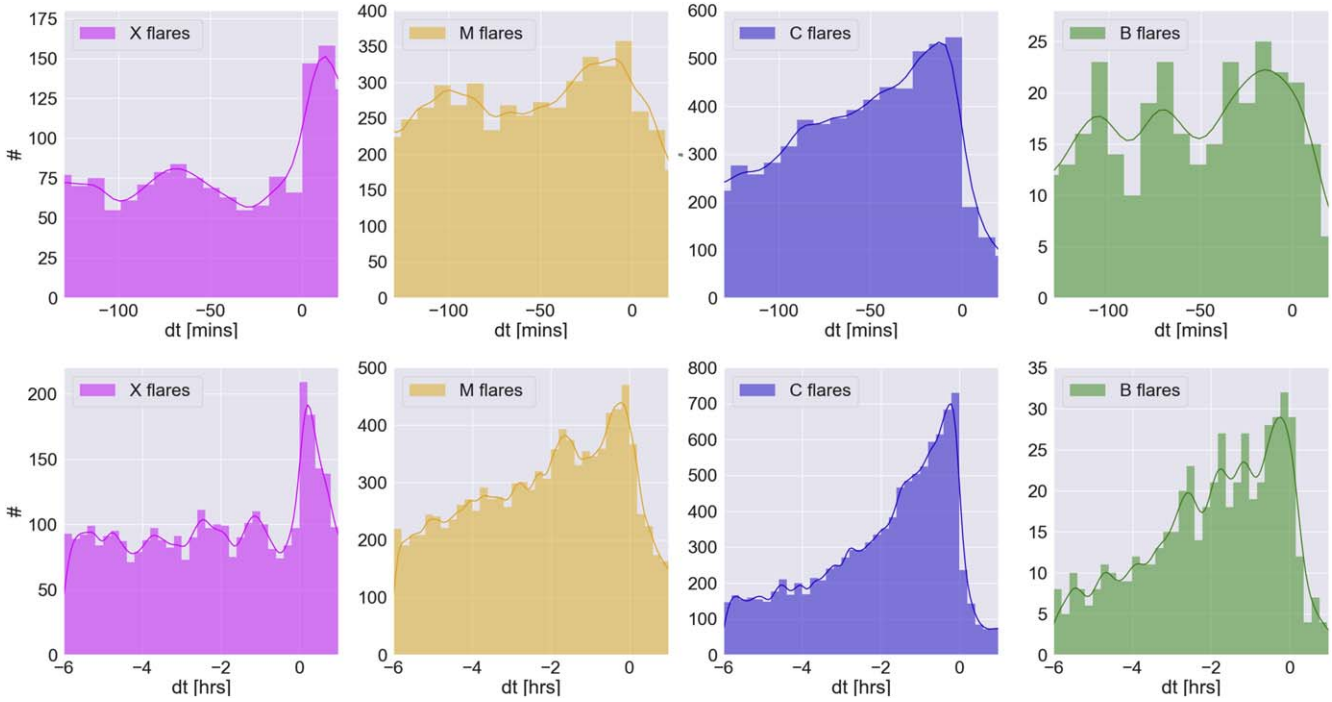

Figure 3. Histograms demonstrating a superposed epoch analysis of EUV signature frequencies before flares. The top and bottom panels show the precursor frequencies 2 and 6 hr before flares, respectively. The different colors signify different magnitude flares, and X-, M-, C-, and B-class flares are shown in the panels from left to right, respectively.

increasing frequency of precursors before the flares except X-class flares. The latter showed a fluctuation, with peaks repeating approximately 1.2 hr apart. Understandably, the highest frequency of EUV signatures were observed at the flare start times. This is due to the fact that main-phase flares are also detected as EUV signatures and are close to the X-ray start times.

5. Conclusions

Previous studies have shown that chromospheric EUV signatures are small-scale magnetic reconnection events that can occur before flares. However, there has not been a large-scale, thorough investigation into the relationship and association between flares and EUV signatures. Using the DEFT detection tool we were able to identify and investigate EUV signatures in flare and no-flare periods. Our primary goal was to explore if EUV signatures occurred consistently before flares, if they could occur without flares, and if flares could occur without EUV precursors. We also investigated differences between EUV signatures based on the flare magnitudes they were associated with.

In 200 days of no-flare data only 38 EUV signatures were detected, i.e., in periods of no flare activity, EUV precursors were only detected 4% of the time when using 6 hr detection windows. We also found that in a database of 360 $\geqslant$C-class flares, only 28 flares had no EUV precursors within 6 hr beforehand. That is, EUV precursors were observed in a 6 hr preflare window 92% of the time. Using the DEFT tool on a combined database of 360 6 hr preflare windows (Study 2) and 360 6 hr no-flare windows (Study 1) produced the following skill scores: HSS (0.88), TSS (0.88), ACC (0.94), BACC (0.94), PRE (0.95), and REC (0.93).

Finally, our last study investigating precursors and post-cursors showed that over 90% of the EUV signatures were associated with $\geqslant$B-class flares and over 50% of all signatures were associated with $\geqslant$M-class flares. We also found that X-class flares showed peak signature frequencies around 1.2, 2.5, and 3.7 hr before the flare start times, with an apparent fluctuation periodicity of $\sim$1.2 hr. M-class flares showed a peak precursor frequency around 100 minutes and a gradually increasing frequency in the last 50 minutes before the flare start time. All magnitude flares showed gradually increasing EUV precursor frequencies before flares except the X-class flares. The latter could be a real phenomenon or simply due to the lower X-class flare sample size. A future study with a larger data size might be able to address this question.

While the discussed results do not yet allow us to forecast flare magnitudes based on individual EUV precursor signatures, the results clearly demonstrate a strong connection between EUV signatures and flares and a significant forecasting potential using EUV signatures. Our next goal is to run DEFT on a large database of consecutive days and calculate the corresponding performance metrics. Furthermore, we are currently transitioning DEFT into real-time use.

Acknowledgments

L.D.K. was supported by the National Science Foundation under grant No. 1931062 issued through the NSF AGS/STR Program. A patent application has been filed by University of Colorado (CU5677B-US1, USPTO SN: 17/985,727). This research was supported in part by the NOAA cooperative agreement NA22OAR4320151. The author thanks Fadil Inceoglu, Paul Lotoaniu, and David Ciplet for the helpful discussions.

ORCID iDs

Larisza D. Krista https://orcid.org/0000-0003-4627-8967

References

Bamba, Y., Kusano, K., Yamamoto, T. T., & Okamoto, T. J. 2013, ApJ, 778, 48
Bamba, Y., Lee, K.-S., Imada, S., & Kusano, K. 2017, ApJ, 840, 116
Bloomfield, D. S., Higgins, P. A., McAteer, R. T. J., & Gallagher, P. T. 2012, ApJL, 747, L41
Cao, W., Gorceix, N., Coulter, R., et al. 2010, AN, 331, 636
Culhane, J. L., Harra, L. K., James, A. M., et al. 2007, SoPh, 243, 19
De Pontieu, B., Title, A. M., Lemen, J. R., et al. 2014, SoPh, 289, 2733
Doswell Charles, A. I., Davies-Jones, R., & Keller, D. L. 1990, WtFor, 5, 576
Fulbright, J. P., Kline, E., Pogorzala, D. R., et al. 2017, Proc. SPIE, 10402, 104020T
Hanssen, A. W. 1965, JApMe, 4, 172
Heidke, P. 1926, GeAnA, 8, 301
Krista, L. D. 2025, ApJ, 978, 121
Krista, L. D., & Chih, M. 2021, ApJ, 922, 218
Kusano, K., Bamba, Y., Yamamoto, T. T., et al. 2012, ApJ, 760, 31
Kusano, K., Iju, T., Bamba, Y., & Inoue, S. 2020, Sci, 369, 587
Leka, K. D., Dissauer, K., Barnes, G., & Wagner, E. L. 2023, ApJ, 942, 84
Lemen, J. R., Title, A. M., Akin, D. J., et al. 2012, SoPh, 275, 17
Nishizuka, N., Sugiura, K., Kubo, Y., Den, M., & Ishii, M. 2018, ApJ, 858, 113
Nishizuka, N., Sugiura, K., Kubo, Y., et al. 2017, ApJ, 835, 156
Pelkum Donahue, K., & Inceoglu, F. 2024, FrASS, 10, 1298609
Schou, J., Scherrer, P. H., Bush, R. I., et al. 2012, SoPh, 275, 229
Su, Y. N., Golub, L., van Ballegooijen, A. A., & Gros, M. 2006, SoPh, 236, 325
Tadikonda, S. K., Freesland, D. C., Minor, R. R., et al. 2019, SoPh, 294, 28
Wang, H., Liu, C., Ahn, K., et al. 2017, NatAs, 1, 0085
Woodcock, F. 1976, MWRv, 104, 1209